Strength of Fault as Infferred from the Stresses Measured in the Vicinity of the Nojima Fault (Extended Abstract)

Kiyohiko Yamamoto[1], Namiko Sato and Yasuo Yabe

Graduate School of Science, Tohoku University, Aramaki-Aoba, Sendai 980-8578

Abstract : The strength of fault is an essential factor for modeling the occurrence process of earthquakes. The stress measurement near faults is the key to know the strength. The Nojima fault in Awaji Is., Hyogo prefecture, Japan, ruptured accompanied by the 1995 Hyogo-ken Nanbu earthquake ($M_{JMA} = 7.2$). *In-situ* stresses have been measured on boring core samples by deformation rate analysis (DRA) for the three sites close to the fault. Two of them locate along the fault segment where surface break is observed. The other is near the southern end of the buried fault extended from the surface break. The stresses have been determined at depths between 310 and 415 m for the two sites in the surface break segment and at depths from 351 to 720 m for the site in the buried fault segment. The stresses show that all the sites are in the strike-slip regime. The largest horizontal stress lies in NW-SE direction for all the sites except for the shallow depths of the site in the buried fault segment. The NW-SE direction is almost consistent with the direction of long-term contraction observed for the Osaka Bay area adjacent to the fault. The stresses seem thus to reflect the regional stress, although they have measured in the vicinity of the fault. It is seen that the direction is almost perpendicular to the fault plane that is nearly vertical. Since DRA is based on the rock property of long-term memory of stress, the stresses measured by DRA are expected to be those before the earthquake. The direction implies thus that the strength of the fault is small, or the fault is weak, although the fault is not of plate boundary. It is the other result that the shear stress is small in the zone within about 100 m from the fault core. The elastic properties are estimated from the measured stresses for the zone on the assumption that the zone is in the post-failure state. The elastic properties suggest that the zone is responsible to the weak strength of the fault.

Key Words : *in-situ* stress, deformation rate analysis, the Nojima fault, weak fault, fractured zone, pressurized fluid.

1. Introduction

It is generally postulated that the majority of the deformation of the earth's crust is due to faulting and that earthquakes occur in the process of faulting, that is, frictional sliding and slip on fault planes. The strength of fault is essential thus for modeling the deformation process of the earth's crust and the criterion or the constitutive relation for frictional sliding is substantial for modeling the process of earthquake occurrence. For the reason, the frictional properties of rocks have been being experimentally and theoretically studied in laboratory. However, it is the most basic for this study to clarify the frictional properties of the faults in nature.

The frictional coefficient of fault is inferred from laboratory experiments to be equal to or more than about 0.6 (*e.g.* Byelree, 1978). On the other hand, the frictional strength for the San Andreas Fault has been inferred to be small from the heat flow data (Brune *et al.*, 1969). The recent data from well borehole breakouts and from hydraulic fracturing measurement appear to support that the San Andreas Fault is weak. The friction coefficient for the fault is estimated to be about 0.1 or so in appearance (Zoback *et al.*, 1987 ; Zoback and Healy, 1992). If this is true, it becomes an important problem whether the small strength is the particular property of the San

Andreas Fault, or the universal property of faults.

It is well known that pressurized pore fluid reduces the compressive or the shear strength of rocks (*e.g.* Handin *et al.*, 1963). In order to explain the discrepancy in the frictional strength between the San Andreas Fault and the simulated faults in laboratories, it is assumed that the pressurized pore fluid is sealed in fault zone (*e.g.* Sibson *et al.*, 1988). Deep drilling was conducted at Cajon Pas in the vicinity of the San Andreas Fault to measure the stresses and the pore fluid pressure at depths in the hole (*e.g.* Zoback and Healy, 1992 ; Coyle and Zoback, 1988). However, they have found neither the evidence for the strength of the fault being normal nor the reservoir for the pressurized fluid.

According to the Byerlee's law, the coefficient of friction is about 0.85 for the small normal stress and about 0.60 for the larger normal stress on a fault plane. The strength of intact rock specimens for compression is approximately represented by the Coulomb's criterion. The criterion is represented to be the sum of the cohesion force and the frictional strength. The frictional strength is expressed as the product of the internal friction coefficient and the normal stress. The internal friction coefficient ranges from 0.5 to 1.5 (*e.g.* Paterson, 1978). This means that the internal friction coefficient is almost comparable in magnitude to the frictional coefficient and that the strength of intact rock specimens is larger only by the amount of the cohesion force. It is known further that the strength of intact rocks decreases with an increase in specimen size (*e.g.* Pratt *et al.*, 1972). Yamamoto (1998, 1999) shows that this size effect cannot be explained without a decrease in the internal friction coefficient with an increase in specimen size. Further, if the frictional strength did not decrease with an increase in specimen size, the frictional strength for faults would exceed the shear strength of intact rocks for large specimens. It should be considered thus that the frictional strength or the friction coefficient for sliding or slip is variable similarly to the strength of intact rock specimens. It may be seen from the above context that the strength of fault is still a problem to be solved.

The strength of fault is defined from the macroscopic viewpoint. The stresses only at a few sites might seem to be insufficient to solve this problem, even if they are the stresses at the sites close to a fault. However, the stresses close to a fault plane are especially important to know the structure of a fault, for example, to know where and how the stresses are relaxed. Further the stress is one of the independent state variables in relation to the strength of fault. The stress measurement is thus almost the only way leading directly to the solution for this problem.

The Hyougo-ken Nanbu earthquake of $M_{\mathrm{JMA}}=7.2$ occurred January 17, 1995. The Nojima fault and the Ogura fault in Awaji, Hyougo prefecture, ruptured accompanied by the earthquake (Awata *et al.*, 1995). These two faults altogether are called the Nojima fault, here. Immediately after the earthquake, Kyoto University (UNV), Geological Survey of Japan (GSJ), and National Research Institute for Earth Science and Disaster Prevention (NIED), respectively, conducted the drillings at Toshima, Ikuha, Hirabayashi, and some sites close to and near the fault. Yamamoto *et al.* (1998) and Sato *et al.* (1999) measured the stresses by deformation rate analysis on the cores of two depths at Hirabayashi (GSJ), three depths at Toshima (TSM) and five depths at Ikuha (GSJ).

Yamamoto *et al.* (1990) and Yamamoto (1995b) have found that rocks have the property of *in-situ* stress memory that is the stress memory of long term. Deformation rate analysis (DRA) has been developed based on the memory as a method for the measurement of *in-situ* stresses. Actually, the stresses can be determined by DRA even from the rock specimens that have been

recovered from depths a few years ago. For the reason, the measured stresses are expected to be the stresses before the earthquake. This paper will review the results by Yamamoto and Yabe (2000) and Sato *et al.* (1999) focusing on the strength of fault, and then try to explain the strength of fault from the elastic properties of fractured zone derived from the stresses measured in the vicinity of the fault.

2. Stresses near the Nojima fault

Sites and Specimens

The 1995 Hyogo-ken Nanbu earthquake ($M_{\text{JMA}} = 7.2$) occurred accompanied by surface rupture more than 10 km long along the Nojima fault. The Nojima fault has the strike of about N45°E and the dip of 80° toward the southeast on an average (*e.g.* Yoshida *et al.*, 1996; Wald, 1996). Awata *et al.* (1995) investigated the trace of the rupture and the amount of the dislocation on the ground surface. Their results are shown in Fig. 1. The right lateral motion is seen to be predominant about twice as much as the reverse motion.

The stress measurements were performed on the boring cores recovered from the holes at Hirabayashi, Toshima and Ikuha close to the fault. Hirabayashi (HRB$_{\text{GSJ}}$) is located in the central part of the Nojima fault, where the largest surface displacement is observed. Toshima (TSM) is located near the southern end of the surface rupture exposed along the fault. The surface rupture was not found around Ikuha (IKH). Ikuha is located about 1 km southeast from the Mizukoshi flexure on the line extended from the fault. According to Satoh and Sugihara (1995), the buried fault reached near the site. The site is inferred to be a few kilometers northeast from the end of the buried fault, referring to the fault estimated from the geodetic and seismological data (*e.g.* Yoshida *et al.*, 1996; Wald, 1996). The sampling sites are at a distance smaller than 50 m from the fault core for HRB$_{\text{GSJ}}$ and at a distance of about 400 m for TSM. The distance is not clear for IKH, but Ito *et al.* (1997) have described that the drill hole intersects a fault around the depth of 670 m.

The rock type of the specimens used in this study is granodiorite except for porphyrite at the two depths of 465 and 639 m of IKH. The Young's modulus of the specimens ranges from about 10 to more than 80 GPa. The specimens of the smallest Young's modulus are of the depth of 639 m at IKH, and those of the largest modulus are of the depth of 310 m at TSM. The inelastic strain was very small for the specimens of the largest Young's modulus and the strain increase is extremely non-linear for the specimens of the smallest modulus. The determination of *in-situ* stresses was hard for both these specimens.

Definition of r-Value

The strength of a fault is expressed in terms of the average normal stress and the average shear stress on the fault plane. On the other hand, the strength of the earth's crust may be defined as the average stress applied to an area in the crust when one of the faults in the area start to rupture to cause the stress drop in the area. The strength of the crust depends thus on the geometry of the fault relative to the applied stress in addition to the strength of the fault. It should be noted that the strength of the crust is permitted to be large, even though the strength of fault is small.

The shear strength of rocks may increase in approximation proportionally to the normal

Fig. 1. a) Location of the sites for the stress measurement by deformation rate analysis (DRA). The arrows indicate the directions of the largest horizontal stress of compression measured at the depths indicated near the arrows. b) The sites indicated in the figure of the surface displacement distribution by Awata *et al.* (1995). The map and the figure are modified from Awata *et al.* (1995).

component of the stress on the maximum shear plane. In order to discuss the stresses in relation to the shear strength of the crust, a parameter r defined by

$$r = (\sigma_1 - \sigma_3)/(\sigma_1 + \sigma_3) \tag{1}$$

is introduced, where σ_1 and σ_3 are the largest and the smallest principal stress of compression. Although the cohesion is neglected in the equation (1), the r value may be thought as an index of the potential of the stress field for shear fracture and has been used as a parameter for the discussion on the potential of stress field for seismic activity and earthquake occurrence. The value of r is calculated here on the assumption that one of the principal directions is in the vertical. If a fault is ruptured at $r=r_s$, r_s may be interpreted as the apparent friction coefficient of the fault, only when the geometry of a fault is near optimal.

Orientation of Stresses

The stresses are summarized in the papers (Yamamoto *et al.*, 1999; or Sato, 2000). The directions θ_{hmax} for the largest horizontal stress of compression are shown in Fig. 1 by arrows. The depths of the measurement are denoted near the respective arrows. Except for shallow depths of IKH, the directions approximately lie in the NW-SE. This direction is almost perpendicular to the fault strike. Since the dip angle of the fault has been estimated to be about 83° near ground surface (Takemura *et al.*, 1997), the shear stress resolved on the fault plane is small, as has been known at Cajon Pass near the San Andreas Fault. Yamamoto and Yabe (2000) have estimated the apparent friction coefficient to be about 0.2 for small depth at TSM, where the r-value is about 0.5.

The directions of the largest horizontal stress at HRB, which might be of the stresses in the fault zone, appear to slightly oppose the right lateral motion of this fault. This may also imply the small frictional stress on the fault. The directions determined by hydraulic fracturing technique are reported to lie in the NW-SE direction, too (Tsukahara *et al.*, 1998; Ikeda *et al.*, 1998). Referring to the horizontal strain between 1885 and 1985 observed by Geographical Survey Institute, Japan (Geographical Survey Institute, 1997), the direction θ_{hmax} is nearly equal to that of the largest contraction of the Osaka bay area adjacent to the sites. This implies that the NW-SE direction for θ_{hmax} has not been formed after the faulting, but suggests that the stress is governed by the tectonic situation even in the vicinity of the fault at least in this case.

The largest and the smallest horizontal stresses (θ_{hmax} and θ_{hmin}) at IKH are plotted for depths in Fig. 2 together with the direction of the largest horizontal stress and the r-value. Sato *et al.* (1999) have found that the direction θ_{hmax} rotates counterclockwise by about 120° or 130° and the r-value is small while the depth increases from 544 m to 720 m. As stated before, it is considered that there is a fault around the depth. The rotation of θ_{hmax} seems to occur near the fault. The direction θ_{hmax} is rather parallel to the fault strike for shallow depth and approximately perpendicular to the strike for larger depth. This direction of NW-SE at the larger depth is almost identical to that reported by Ito *et al.* (1997) and to those at the other sites.

Distribution of r-Value

TSM is in the strike-slip regime, but compression is slightly predominant. The r-values are determined at about 0.5. This means that the r-value has reached to 0.5 at least in a region in the vicinity of the fault at the faulting, while the frictional coefficient of the fault is about 0.2. Tsukahara *et al.* (1998) performed the hydraulic fracturing measurement at two depths near 1,500 m. The stresses at these depths are of almost pure strike-slip regime. The r-values at the depths are calculated to be about 0.16. They are significantly small compared with those at the small depths obtained by DRA.
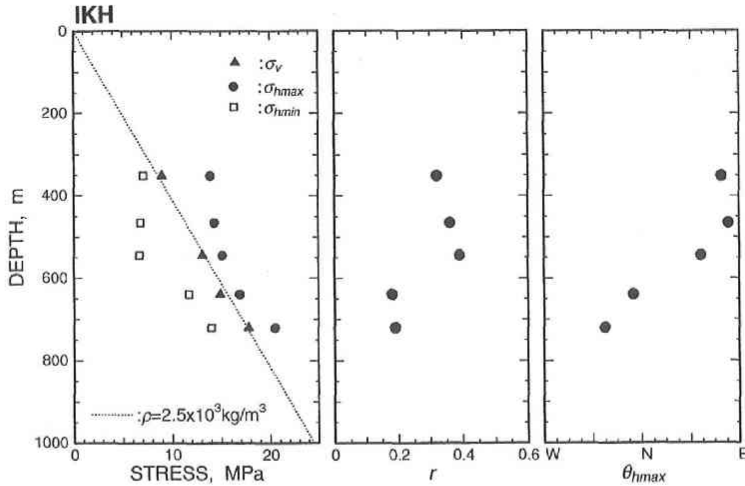
Fig. 2. Stresses plotted for depths for IKH. a) The vertical, the largest and the smallest horizontal stress. b) r-value, and c) the direction of the largest horizontal stress θ_{max}. (Data after Sato *et al.*: 1999)

Ikeda *et al.* (1998) carried out the hydraulic fracturing measurement in a hole (HRB_{NIED}) near HRB_{GSJ} drilled by NIED. Their measurement revealed that the site is in the reverse fault regime. The largest horizontal stresses appear to be close in magnitude to those at the depths of about 300 and 400 m of TSM, although the type of stress field for the depth is different. On the other hand, the stresses at depths near 1,200 m are in the strike slip regime. The r-values calculated for their results at HRB_{GSJ} are between 0.3 and 0.4 for the depth smaller than about 800 m and nearly equal to or smaller than 0.2 for the depth near 1,200 m. The characteristics of the small r-value and the strike-slip regime for the depth near 1,200 m are quite similar to those at the large depths of TSM.

Sato (2000) obtained the stresses around 350 m in depth for HRB_{GSJ} by DRA. The stresses are characterized with the strike slip regime and the relatively small r-values. These characteristics are different from those at shallow depths of HRB_{NIED}, but rather similar to those at greater depths of HRB_{NIED} and TSM. The HRB_{GSJ} hole locates approximately at a distance of about 50 m, while HRB_{NIED} at a distance of about 400 m from the fault core on ground surface. The location of the site relative to the fault core makes us to suspect that the r-value depends not on the depth but on the distance from the fault core. The small r-value may be caused not by the stress drop due to the faulting this time, because the r-values by DRA are considered to be of the stresses before the earthquake.

Sato *et al.* (1999) have found for IKH that the r-value is small at 639 m and 720 m in depth. They have further pointed out that θ_{hmax} and θ_{hmin} are almost constant without regards to depth at shallow depths and θ_{hmax} at shallow depths are almost equal to θ_{hmin} at larger depths. As described before, there is an estimated fault around 670 m in depth. The decrease in the r-value together with the rotation of stress orientation described before probably reflect the property of the zone in the vicinity of the fault.

Ito (1996), Ikeda *et al.* (1998), and Shimazaki *et al.* (1998) presented the trajectories of the boreholes of HRB_{GSJ}, HRB_{NIED}, TSM, respectively, in relation to the fault core, as shown in Fig.
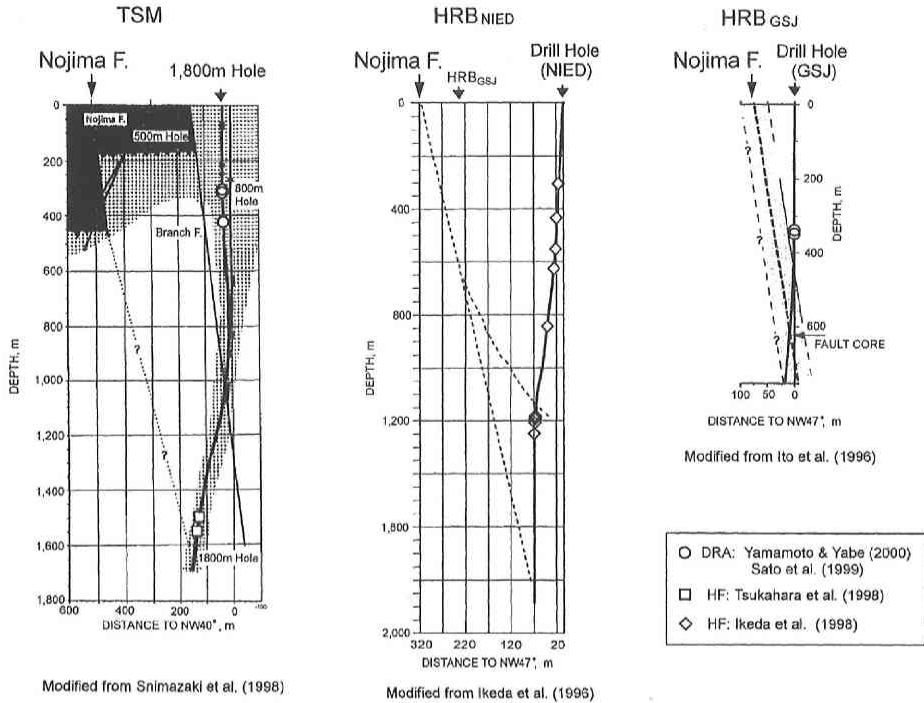
Fig. 3. Points for the stress measurements on the trajectories of drill holes. The points are indicated by symbols. The different symbols denote the different methods of the stress measurements. The dot lines or dash lines indicate the inferred fault plane of the Nojima fault. The left figure is of Toshima hole (TSM) after Shimazaki *et al.* (1998), the center of Hirabayashi hole by NIED (HRB$_{NIED}$) after Ikeda *et al.* (1996), and the right of Hirabayashi hole by GSJ (HRB$_{GSJ}$) after Ito *et al.* (1998).

3.   The distances of the measuring points from the main fault core are known from the trajectories.   Sato (2000) showed the relationship between r-value and the distance.   The relationship is shown in Fig. 4 together with the relationship to the depth.   The small shear stress near the core is clearly seen in this figure.   It may be thus reasonable to conclude that the small shear stress is caused not by the change in the stress with the depth but by the distance from the main fault core (Sato *et al.*, 1999).   The small magnitude of shear stress may be one of the characteristics of the stress state in the zone close to the fault core.   The width of the zone of small r-value is about 100 m in the present study.

According to Yamamoto *et al.* (1997), the r-values are around 0.3 for the areas of moderate seismic activity.   The r value larger than 0.4 has been observed near the epicenter of 1984 Nagano-ken Seibu Earthquake (M$_{JMA}$=6.8) (Yamamoto *et al.*, 1990).   The large r-value of about 0.5 at TSM together with those for 1984 Nagano-ken Seibu earthquake imply that there are the areas in focal region, where the r-value is large independently of friction coefficient of fault.
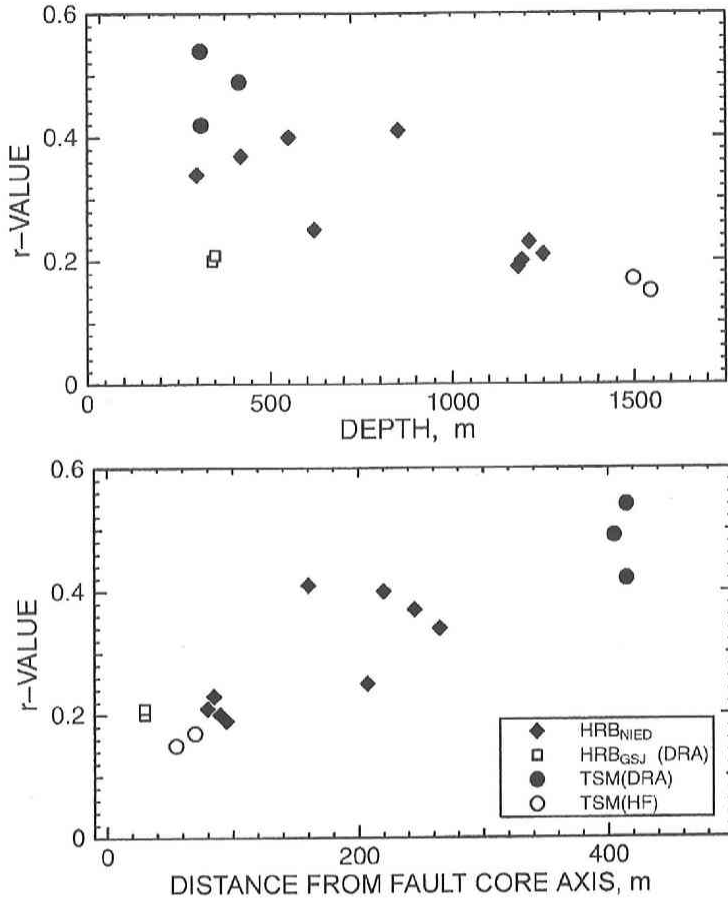
Fig. 4.   The values of r plotted for the depth (upper) and for the distance from the fault core axis (lower).   The difference in symbol denotes the difference in the site and the method of measurement (After Sato : 2000).

3.   Role of Fractured Zone on The Strength of Fault

Definition of Fractured zone

The r-value is small in the zone within about 100 m from the fault core as seen in Fig. 4. Although the r-value has been introduced to represent the potential for generating shear fracture, this small r-value may not mean the low potential for earthquake occurrence.   Referring to the study by Chester *et al.* (1993), large strain has been concentrated near the fault core.   It may be reasonable to consider that the small r-value is resulted from the zone that has been fractured and has lost the ability to support the load.   The zone is called fractured zone, hereafter.   The width of the fractured zone may be smaller than the width of the small r-value zone.

Since the stresses measured by DRA are considered to be those before the earthquake, it may be reasonably supposed that the fractured zone has grown up before the faulting at this time. The stress state in the fractured zone is schematically illustrated in Fig. 5a).   The largest principal stress directs almost perpendicularly to the fractured zone in order to contract the zone. Chester *et al.* (1993) have pointed out that the strain in fault zone may be modeled as simple shear
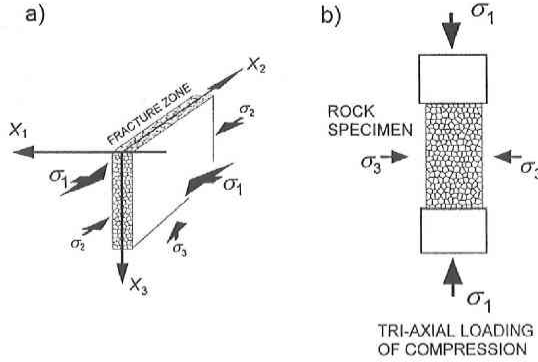
Fig. 5.   a) Schematic illustration for the stress state in a fault zone.   The coordinate taken for the fault is also shown.   The x_3 is approximately equal to the depth direction in the case of the Nojima fault.   The notation σ_i indicates the principal stress of compression, provided $\sigma_1 > \sigma_2 > \sigma_3$ ($\sigma_3 > \sigma_2$ in the case of the Nojima fault). b) A rock specimen under loading of tri-axial compression simulating the fractured zone.

in the core of the fault and nearly fault normal contraction in the surrounding damaged zone and host rock.   Without the simple shear zone at the fault core in their model, the present feature of the fractured zone may be consistent with their model.   The r-value is large comparably to the fracture strength of rocks outside the zone.   Taking this large r-value together with the stress orientation, it is reasonable to consider that the rock specimens under tri-axial loading of compression can simulate the rocks in the fractured zone, which have been so damaged as to lose the ability to support the lord.

Fracture Density and Tensile Crack Density

Here, let us define the Cartesian coordinate so that x_1 lies in the direction perpendicular to the loading axis, as shown in Fig. 5b), and assume that cracks orient their surfaces parallel to x_1 and distribute their normals symmetrically around x_1.   According to Yamamoto (1995a, 1998), for a rock specimen of a kind of granite under tri-axial compression with confining pressure σ_3, the density c of tensile cracks is expressed by

$$c = Cf(\sigma_3)G(u) \qquad \text{for } 0 \leq G(u) \leq 1. \tag{2}$$

Here, c is defined by

$$c = \phi/a.$$

ϕ and a, respectively, are porosity and aspect ratio of cracks. $f(\sigma_3)$ is a function proportional to $\sigma_3^{-1/2}$.   The function $G(u)$ represents the density of shear micro-fractures or the fracture density and is expressed by

$$G(u) = s_0[u/(1-G(u))]^m, \tag{3}$$

s_0 being the normalization factor.   Here, the fracture means the loss of the ability to support the applied load.   The normalized shear stress u is defined by $u \cong r/r_f$, where r is given by (1). r_f denotes the shear strength of a rock specimen and the equality holds when the cohesion can be neglected in the Coulomb criterion.   When $f(\sigma_3)$ is taken to be unity at $\sigma_3 = 0.1$ GPa, C has been determined to be approximately 10.   The expressions (2) and (3) imply that the stress concentra-
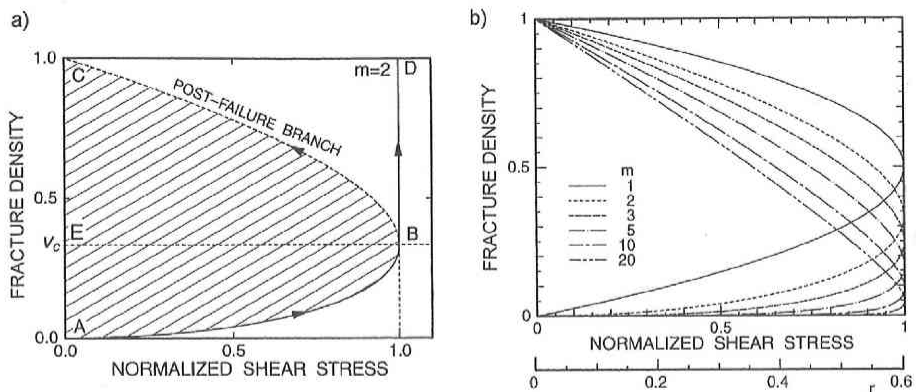
a)

b)

Fig. 6.   The fracture density $G(u)$ as the function of applied shear stress u normalized
by the macroscopic strength.   a)   Explanation of $G(u)$.   The stress at the point
B means the macroscopic fracture strength. The path BD means the macroscopic
fracture that all the volume of specimen loses the strength at once.   The path BC
means the post-failure state.   b)   The behavior of the function for some values
of m. r is defined by Eq. (3) in the text.

tions due to shear fracture keep the tensile cracks open.

The behavior of $G(u)$ is schematically illustrated in Fig. 6a). Speaking in more detail, the value of G can be interpreted as the fraction of the volume in a specimen that has lost the strength by fracturing.   The function $G(u)$ yields the upper and the lower bound of the fracture density in order that specimens are stable for the applied stress u.   Specimen can be stable thus for the values of (u, G) in the hatched area enclosed by the curve ABC and the line CA in Fig. 6a).   The stress u at the point B is the largest stress the specimen can support or the fracture strength of the specimen.   Therefore, the state in the upper part of the zone over the line EB cannot ordinarily be achieved.   The state especially on the line denoted by BC is called here the post-failure state.   This state can be exactly realized in laboratories only when a completely rigid apparatus is used to apply displacements to a specimen.

The value of G increases tracing the curve AB with an increase in $u \approx r/r_f$ or r when G is smaller than the critical fracture density v_c.   When G is larger than v_c, the stress in the specimen cannot exceed the value of u on the curve BC at a given value of G.   When a value of u is obtained for a specimen in the post-failure state by observation, the value of G calculated for the value of u using (3) is the largest estimation of the fracture density G.   The largest of the density c of tensile cracks in the specimen may be estimated thus for the measured shear stress r by making use of (2) and (3).

Estimation of Tensile Crack Density in the Fractured zone

As stated before, since the strain produced in the zone close to the fault core may be much larger than that elastically supportable, the stress in the zone may be the largest stress the zone can support.   It is reasonable thus to suppose that the rocks in the fractured zone are in the post-failure state.   It is assumed further that the expression (3) is applicable throughout the range of fracture density G.   Although this expression has been experimentally confirmed to hold for specimens before the macroscopic fracture, this assumption may be valid for the curve BC that means the values of G larger than v_c, because both curves AB and BC have been derived from

a single model.

On the assumptions above, if the stress r is determined by observation for the fractured zone, the largest value of G expected for the zone can be estimated for $u = r/r_f$. Figure 6b) shows the function $G(u)$ calculated for some values of parameter m. The value of m has been estimated to range from 5 to 10 for some kinds of rocks and the crust (Yamamoto, 1998). Assuming that the shear strength of the rocks that are free from flaws, or the rocks outside the fractured zone, is represented by $r_f = 0.6$, the fracture density $G(u)$ is estimated at a value between 0.75 and 0.85 for r between 0.16 and 0.2 that has been obtained for the fractured zone. The density c of tensile cracks is thus estimated to be between 7.5 and 8.5 in the fractured zone.

Estimation of Elastic Constants of The Fractured zone

The density of tensile cracks has been estimated above. The elastic constants can be theoretically calculated for the estimated crack density by the method that is based on the theory of Eshelby (1957). The cracks in the composites modeled by Eshelby are isolated from one another. In the case of the fluid-saturated cracks, the fluid in the cracks may be pressurized when the composite is deformed. It is thus a problem how to think about the behavior of the fluid, when the Eshelby's model is applied to fractured zone.

Even if fractured zone is permeable, it needs a time for the fluid to transfer from a crack to other cracks. The fluid may be pressurized thus for the dynamic deformation of the zone such as caused by seismic waves, while the cracks may behave as if they are void for the quasi-static deformation of the zone over a long period of years. For the reason, the elastic constants will be calculated here in both the cases that the cracks in the fractured zone are void and that the cracks are saturated with water. The former case is for the discussion on the strength of faults and the latter is for the discussion on the velocities of the elastic wave propagation.

The composites that contain randomly oriented inclusions in isotropic matrix are called isotropic composites. For the isotropic composite containing spheroidal inclusions, the elastic constants can be exactly calculated by differential scheme (DS: Roscoe, 1952) or new self-consistent scheme (NSC: Salganik, 1973; Yamamoto et al., 1981), provided that cracks are permitted to statistically intersect one another. However, the method actually required is for the calculation of the constants of anisotropic composites, because the crack orientation has been provided to be preferred to some directions in fractured zones. Nishizawa (1982) calculated the elastic constants for anisotropic composites by NSC. However, the calculation seems to be not easy in practice in the case that cracks are arbitrarily oriented. Yamamoto (1981, 1995) proposed a method called weak interaction approximation (WIA) to calculate the approximate values of the constants for anisotropic composites whose matrix is isotropic. Here, the elastic constants of the fractured zone are estimated making use of WIA.

a. In the case of randomly oriented cracks

Firstly, the elastic constants of isotropic composites will be introduced here for the two purposes. One of them is for the overview of the elastic constants of the fractured zone and the other is as the reference for the elastic constants calculated by WIA. The effective incompressibility and the effective rigidity of an isotropic composite calculated by both the methods are shown in Fig. 7. In the case of water-saturated cracks, it is seen that both methods yield the almost the same elastic constants throughout the range of crack density to about 8. Although
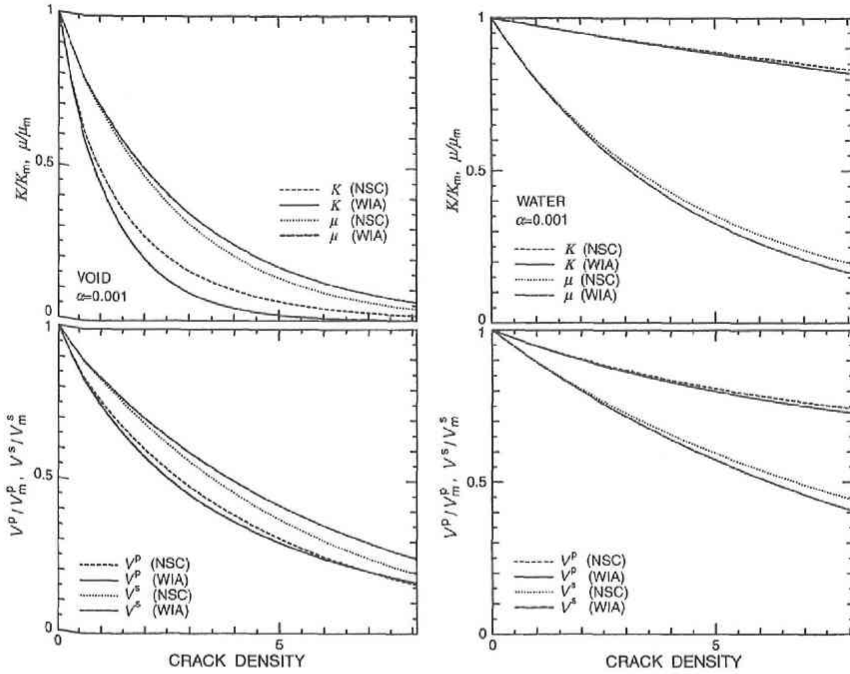
Fig. 7.   The changes in effective elastic property with crack density for isotropic
composites.   The results calculated by WIA are compared with those by NSC.
The upper figures show the relationships for effective incompressibility and
effective rigidity, the lowers for the P- and the S-wave velocity.   The left figures
show the case of void cracks and the left ones for water-saturated cracks.   The
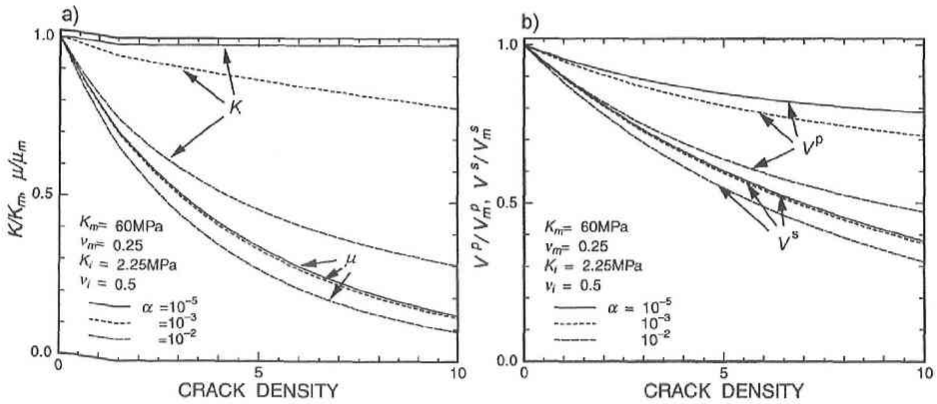Poisson's ratio of matrix is taken to be 0.25.

Fig. 8.   Effective elastic constants and elastic wave velocities of isotropic composites
calculated as the functions of crack density.   Aspect ratio of cracks is taken as
a parameter.   Randomly oriented cracks are included in isotropic matrix.   a)
Incompressibility K and rigidity μ, b) P- and S-wave velocities.

the difference between WIA and NSC appears to be large in the case of void inclusions, it is seen
that the characteristics in the relationships among the elastic constants are well approximated by
WIA.   The method of WIA is considered thus to be sufficient for the rough estimation of the

elastic properties of fractured zone even in the case of void inclusions.

The relationships between effective elastic constants and crack density depend on the shape, or the aspect ratio, and the elastic property of cracks. Figure 8 shows the effective elastic constants of isotropic composites calculated by NSC for the aspect ratio as a parameter in the case of water-saturated cracks. In this figure, it is seen that when aspect ratio is small, the decrease in the incompressibility with an increase in the crack density is small compared with that in the rigidity. However, this property does not hold true when the aspect ratio becomes larger. It is also seen in Fig. 7 that the incompressibility decreases with an increase in crack density similarly to the rigidity when cracks are void. These means that large incompressibility for small aspect ratio is caused by the water pressurized in the cracks that are isolated from the outside of the composite. It may be concluded that if the crack orientation is random, the amounts of decrease in the incompressibility and the rigidity may be almost the same with an increase in crack density, when the composite is slowly deformed. It should be noted that this is not the case of the fractured zone, because the zone is subjected to the larger stress in the direction close to the fault normal.

b. *In the case of cracks in preferred orientation*

The Cartesian coordinate has been defined so that x_1 directs perpendicularly to the fault plane, as shown in Fig. 5a), and assume that cracks in the fractured zone orient their surfaces parallel to x_1 and distribute their normals symmetrically around x_1. The Young's modulus E_{ii} and the rigidity μ_{ij} of the zone are calculated by making use of WIA. Here, E_{ii} denotes the stiffness between the longitudinal strain e_{ii} and the normal stress τ_{ii}, and μ_{ij} does the stiffness between e_{ij} and τ_{ij}. Figure 9a) shows the constants of the composite with the void cracks (void crack model) and Figure 9b) does the constants of the composite with water-saturated cracks (saturated crack model), the elastic constants and the elastic wave velocities are shown for the aspect ratios of 0.001 and 0.01. As stated before, the void crack model and the saturated crack model respectively are considered to approximate the response for the quasi-static deformation and for the dynamic deformation of fractured zone.

If the normal stress and the shear stress on the fault plane are responsible to the strength of fault, E_{11} and μ_{13} $(=\mu_{12})$ are important for the strength. It is seen in Fig. 9 that the differences in E_{11} and μ_{13} between void-crack model and saturated crack model are not found, while E_{33} and μ_{23} for saturated crack model are larger than those for void-crack model. It may be said that the effective elastic constants responsible to the strength of fault have only small dependence on the existence of water in fractured zone. The amount of the decrease in Young's modulus E_{11} with an increase in crack density is smaller than 10% of the Young's modulus of the host rock even for the aspect ratio of cracks equal to 0.01, while the amount of decrease in the rigidity μ_{13} is larger than 85% of that of the host rock when the density of tensile cracks is larger than 7.5.

The notation V_{ij} denotes the velocity of the waves propagating to the x_i direction with the motion in the x_j direction. The velocity V_{11} of P-waves propagating to the x_1 direction shows only a small decrease with an increase in crack density, whether or not the cracks are saturated with water. Its dependence on the aspect ratio is also small. The velocity V_{13} of the S-waves propagating along the fault strike with the motion direction vertical to the fault plane is independent of the water saturation. Further, the velocities V_{13} and V_{23} of the S-waves are less dependent on the aspect ratio of cracks. These wave velocities are considered to be useful to
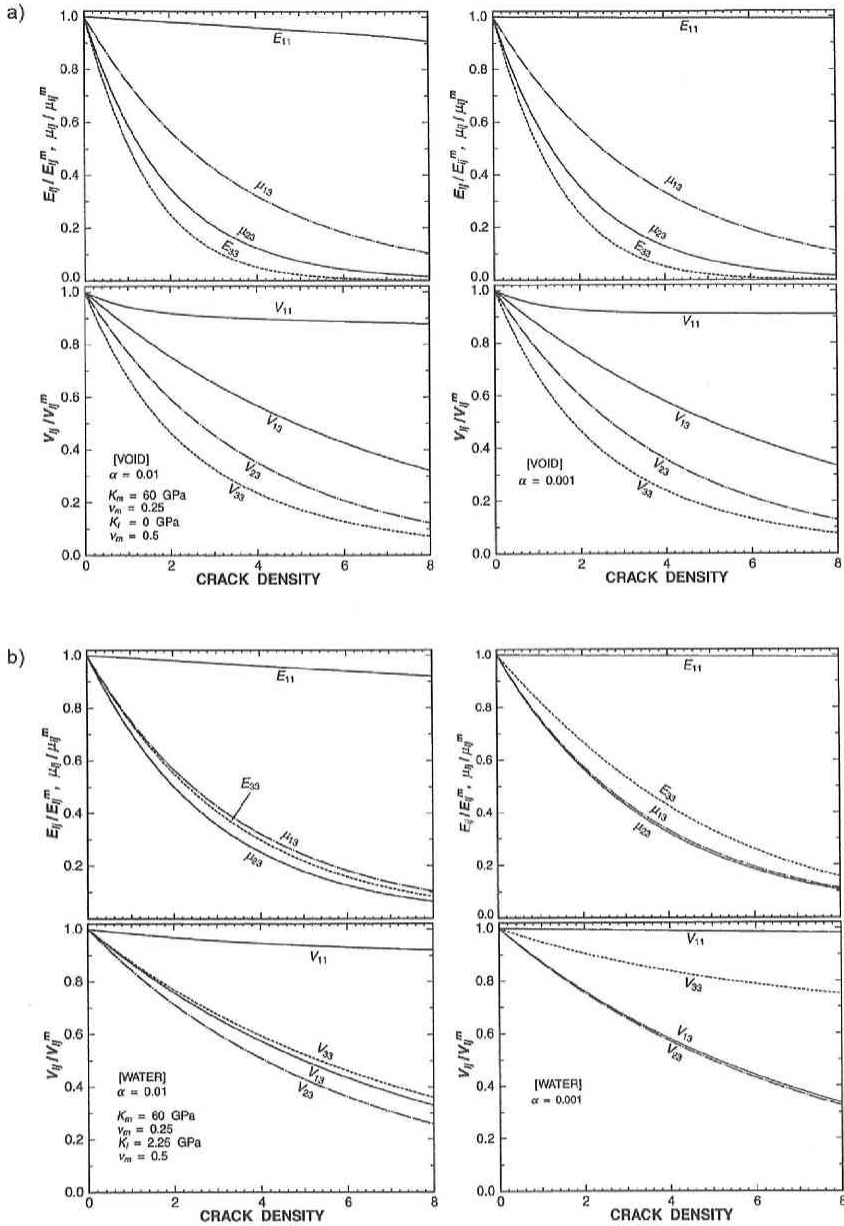
Fig. 9. Effective elastic constants (upper) and elastic wave velocities (lower) of fractured zone calculated as the functions of crack density. The Cartesian coordinate is taken as shown in Fig. 5a). Young's modulus E_{ii} is for the normal stress and rigidity μ_{ij} for the shear stress in x_j direction on the plane whose normal is in the x_i direction. The cracks in the fractured zone orient their surfaces parallel to x_1 and distribute their normals symmetrically around x_1. The left figure shows the cases of $\alpha=10^{-2}$, the right does the case of $\alpha=10^{-3}$. a) Void cracks, b) Water-saturated cracks.

know the structure of fractured zone relating to the mechanical property of the zone. The velocities of the other components of waves may show more complex behaviors. It is seen in Fig. 9 that the velocities V_{13} and V_{23} of the S-waves decrease to about 35 to 40% of those of the host rock.

Kuwahara and Ito (1999), and Nishigami (2000) estimated the width and the elastic property of fractured zone from the elastic waves guided by the zone. According to them, the width of the fractured zone is about 20 to 50 m and the velocity of S-waves is 40 to 66% of the velocity outside the zone. These are the results of the analysis performed on the assumption of the isotropy of the fracture zone and the results may include the tradeoff between the width and the velocity. The focused depths may be different between the analysis of the guided waves and the present stress measurement. Regardless of these differences and the incompleteness of the assumptions in both studies, both the results are seen to be very close to each other. This coincidence implies that the present assumption, that is the fractured zone is in the post-failure state, is justifiable.

A Model for Weak Fault

The stress field should have moved to the lithostatic state in the fractured zone that is in the post-failure state. This may be a reason that one of the principal axes of stress becomes nearly perpendicular to the fault plane at least in or near the fractured zone. Therefore, this perpendicularity does not always mean weak fault. It is hypothesized here that the fault with such fractured zone is weak. In order to certify this hypothesis to be valid, it is necessary to discuss the response of the fractured zone to the change in the stress applied to the fault. For this discussion, let us consider a fault that is completely locked. It is not necessary for this fault to take the frictional stress into consideration. Considering a region including such a fault and the average shear stress on a plane parallel to the fault in the region, the strength of the fault means the average shear stress at the time when a shear rupture propagates all over the fault in the region. This is identical to the shear strength of the region, in which the fault is included as a flaw. Here the response of the fault zone will be discussed when the shear stress and the normal stress on a plane parallel to the fault plane are applied to the region.

An image for a segment of a fault is shown in Fig. 10. There may be in fault zone the asperities and the apertures. In the asperity, the surfaces of both sides of the fault contact with each other. It is assumed for simplicity that the effect of the geometry of asperities on the stress concentration can be neglected. In the case that the apertures are void or saturated with unsealed fluid, the average normal stress σ_c in the asperities in Fig. 10 may be written as

$$\sigma_c = \sigma_n / S, \tag{4}$$

σ_n being the applied normal stress averaged over the fault plane and S (≤ 1) the fraction of the area occupied by asperities in the total area of fault plane. If the strength of asperities is assumed to obey the Coulomb's criterion for failure, the strength of fault τ_s may be expressed by

$$\tau_s = S\sigma_0 + \mu S\sigma_c, \tag{5}$$

where σ_0 and μ are the cohesion and the internal friction coefficient of the asperities. Therefore, when S is small, the shear strength τ_s of the fault is expressed by
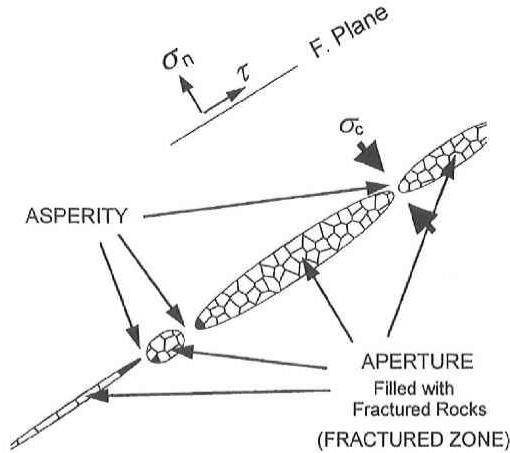
$$\tau_s \approx \mu\sigma_n. \tag{6}$$

Fig. 10.   Conceptual illustration of the horizontal cross-section for a vertical fault. Asperity means the part of a fault plane where the surfaces of both blocks completely contact with each other.   The fractured zone is the aperture filled with fractured rocks. σ_n and τ denote the average normal stress and the average shear stress applied to the plane parallel to the fault plane. σ_c indicates the normal stress in asperity areas.

This expression appears to be corresponding to the Byerlee's law and the strength is seen to be independent of S.   This may be a rough explanation for the frictional strength that is approximately constant independently of contact area.

Consider the case that the apertures are filled with completely incompressible material with negligibly small rigidity for simplicity, as illustrated in Fig. 10.   In this case, the normal stress in the asperities is not expected to change with the change in the fraction S of the area of asperities, while the shear stress τ_c in the asperities builds up with a decrease in the fraction S.   The strength τ_s of fault is thus written as

$$\tau_s \approx S(\sigma_0 + \mu\sigma_n). \tag{7}$$

The strength τ_s decreases with a decrease in the asperity area S or an increase in the aperture area.   As previously described, the rigidity of fractured zone decreases to about 10 or 20 % of those of the matrix, while the Young's modulus in the direction perpendicular to the fault plane is close to that of the host rocks.   This may imply that the shear deformation of fractured zone, which is larger than the contraction, makes the strength of fault decrease.   The elastic property and the structure of fractured zone may be important thus for the strength of fault.

The shear strength of fault may decrease with an increase in the segments with fractured zone as seen from the above.   This is considered to be one of the possible mechanisms for weak faults.   Pressurized pore fluid is not necessarily required for the explanation of weak fault in this model.   Actually, pressurized fluid has been observed in fractured zone neither for the Nojima fault nor for the San Andreas Fault.

4.   SUMMARY

The Nojima fault in Awaji, Hyogo prefecture, Japan, ruptured accompanied by the 1995

Hyogo-ken Nanbu earthquake ($M_{JMA} = 7.2$). The *in-situ* stresses in the vicinity of the fault have been measured by the method of deformation rate analysis (DRA) about one year after the earthquake. This method is based on the rock property of *in-situ* stress memory of long term. Therefore, the stresses obtained by the method are expected to be those before the earthquake.

The measurements have been performed for 343 and 350 m in depth at Hirabayashi (HRB), 310, 312, and 415 m in depth at Toshima (TSM), and 5 depths from 351 to 720 m at Ikuha (IKH) sites. HRB and TSM locate along the fault segment of large dislocation observed on the ground. IKH is near the southern end of the buried fault extended from the Nojima fault. The stresses are in the strike-slip regime for all the sites. The maximum horizontal stress lies in the NW-SE direction at HRB and TSM. The direction at IKH rotates counterclockwise by about 120° or 130° with an increase in depth from 544 m to 720 m. The direction at 720 m depth is almost identical to that for the other sites. The NW-SE direction is almost perpendicular to the fault plane and is consistent with that obtained by hydraulic fracturing technique after the earthquake. The rotation of the direction of the largest horizontal stress occurs near a buried fault.

The estimated stresses are considered to be the stresses before the earthquake. The fault plane is nearly vertical. The direction of the largest horizontal stress suggests thus that the shear stress on a fault plane is very small even before the earthquake. The direction of NW-SE is close to the largest contraction direction during about 100 years obtained for the adjacent area by the geodesic survey. The results support the concept that the fault is a preexisting weak plane.

Defining r value as the maximum shear stress divided by the normal stress on the maximum shear plane, the values are large at the depths smaller than about 500 m for the sites except for HRB_{GSJ}. The values at the depths around 350 m of HRB_{GSJ} are small. The small values have been obtained also at great depths for TSM and HRB_{NIED} by hydraulic fracturing technique. It can be inferred from these data together that the small r-value is not caused by the reason of the depths of the measuring points but of their small horizontal distance from the fault core. The small r-values are obtained for the points at the distances within 100 m from the fault core.

This small r-value near the fault core may reflect the stress in the fractured zone. In the fracture zone, the shear stress is small, while the shear strain is concentrated. This means that the zone has lost the ability to support a large shear stress due to the large fracture density or the zone is in the post-failure state. This may be a reason that shear stress on the fault plane is small or one of the principal axes of stress is nearly perpendicular to the fault plane.

When the zone is in the post-failure state under stress of compression perpendicular to the fault plane, the elastic constants of the zone can be estimated by making use of the knowledge about the fracturing process of rock specimens under tri-axial loading of compression. The rigidity thus estimated is smaller than 20% as much as that of the host rock, while the Young's modulus is more than 90% of that of the host rock. The S-wave velocity corresponding to this rigidity is almost equal to that obtained from the elastic waves trapped in the fractured zone. This implies the validity of the interpretation that the fractured zone is in the post-failure state under the stress of compression almost perpendicular to the fault plane.

The property of the small rigidity compared with the Young's modulus is expected for the fractured zone. If it is assumed that a fault consists of apertures filled with fractured rocks or fractured zone segments and asperities or completely contact areas, the property of fractured zone described above may not increase the normal stress at asperities or the shear strength of

asperity but produce high concentration of shear stress at the asperities.   This effect may make the fault weak.   It is considered thus that the property of fractured zone is responsible to weak faults.   The pressurized fluid may not be essential for weak faults in this context, though the pressurized fluid might play an important role on the propagation of rupture.

References

Awarta, Y., K. Mizuno, Y. Sugiyama, R. Imura, K. Shimokawa, K. Okumura and E. Tsukuda, 1996 : Surface fault ruptures on the northwest coast of Awaji Island associated with the Hyogo-ken Nanbu Earthquake of 1995, Japan, *Zisin 2*, **49**, 113-124 (in Japanese with English abstract).

Brune, J.N., T.L. Henyey and R.F. Roy, 1969 : Heat flow, stress and rate of slip along the San Andreas fault, California, *J. Geophys. Res.*, **74**, 3,821-3,827.

Byerlee, J., 1978 : Friction of rocks, *Pure and Appl. Geophys.*, **116**, 615-626.

Geographical Survey Institute, 1997 : The horizontal strain in Japan, 1994-1883, *Geographical Survey Institute* (Maps).

Chester F.M., J.P. Evans and R.L. Biegel, 1993 : Internal structure and weakening mechanisms of the San Andreas fault, *J. Geophys. Res.*, **98**, 771-786.

Coyle B.J. and M.D. Zoback, 1988 : In situ permeability and fluid pressure measurements at ~2 km depth in the Cajon Pass research well, *Geophys. Res. Lett.*, **15**, 1,029-1,032.

Handin, J., R.V. Hhager, Jr., M. Friedman and J.N. Feather, 1963 : Experimental deformation of sedimentary rocks under confining pressure : Pore pressure tests, *Bull. Am. Soc. Petrol. Geol.*, **47**, 717-755.

Ikeda, R., Y. Iio and K. Omura, 1998 : Scientific drilling and in-situ stress measurements in the vicinity of active faults, *Chikyu Manthly, Suppl*, No. 21, 91-96 (in Japanese).

Ito, H., 1997 : Structure and physical properties of the Nojima fault, *Proc. Symp. on Drilling Project of Faults*, (ed.) Shimazaki, Kyoto Univ., 37-59.

Ito, H., Y. Kuwahara and O. Nishizawa, 1997 : Stress measurements by the hydraulic fracturing in the 1995 Hyogoken-nanbu earthquake source region, In K. Sugawara and Y. Obara (ed.), Rock Stress, A.A. Balkema., 351-354.

Kuwahara, Y. and H. Ito, 1999 : Deep structure of the Nojima fault by trapped wave analysis, *Proc. Int. W / S on the Nojima fault core and borehole data analysis*, Nov. 22-23, Tsukuba, Japan, (GSJ Interim Rep. No. EQ/00/1 : USGS Open-file Rep. 00-129), 283-289.

Nishigami, K., 2000 : Investigation of deep structure of active faults using scattered waves and trapped waves, Seismogenic Process Monitoring, (eds.) Ogasawara, Yanagidani & Ando, Balkema, Rotterdam, in press.

Nishizawa, O., 1982 : Seismic velocity anisotropy in a medium containing oriented cracks—Transversely isotropic case, *J. Phys. Earth*, **30**, 331-347.

Paterson, M.S., 1978 : Experimental rock deformation-Brittle Field, *Springer-Verlag*, pp. 254.

Pratt, H.R., A.D. Black, W.S. Brown, and W.F. Brace, 1972 : The effect of specimen size on the mechanical properties of unjointed diorite, *Int. J. Rock Mech. Min. Sci.*, **9**, 513-529.

Roscoe, R., 1952 : The viscosity of suspensions of rigid sphere, *British Journ. Appl. Physics*, **3**, 267-269.

Salganik, R.L., 1973 : Mechanics of bodies with many cracks, *Mekh. Tverd. Tela (Mech. Mats.)*, **8**, 135-143.

Sato N., 2000 : Estimation of stresses in the vicinity of the Nojima fault from rock core samples, *Master thesis*, Tohoku University, pp. 87 (in Japanese).

Sato N., Y. Yabe, K. Yamamoto, and T. Hirasawa, 1999 : Stresses at sites close to the Nojima carthquake

fault estimated from core samoles: III, *Prog. Abst. Seism. Soc. Japan*, 1999 Fall Meeting, C14. (in Japanese)

Satoh, T., and M. Sugihara, 1995: A GPS survey of triangulation points for crustal deformation associated with the 1995 southern Hyogo prefecture earthquake, *Chishitsu News*, No. 490, 41-43 (in Japanese).

Shimazaki,K., M. Ando, K. Nishigami, and N. Oshiman, 1998: Water injection test at Ogura site along the Nojima earthquake fault, *Chikyu Manthly, Suppl*, No. 21, 33-37 (in Japanese).

Sibson, R.H., F. Robert and K.H. Poulsen, 1988: High-angle reverse faults, fluid-pressure cycling, and mesothermal gold-quartz deposits, *geology*, **16**, 551-555.

Takemura K., A. Murata, T. Miyata, A. Lin, and T. Sotoda, 1997: Description on the cores recovered by drilling, *Proc. Symp. on Drilling Project of Faults*, (ed.) Shimazaki, Kyoto Univ., 115-125 (in Japanese).

Tsukahara, H., R. Ikeda, and K. Yamamoto, 1998: In-situ stress measurement at points close to Nojima fault at the depths about 1500m—The maximum compressive stress perpendicular to the fault strike-, *Chikyu Manthly, Suppl.*, No. 21, 66-69 (in Japanese).

Wald, D.J., 1996: Slip history of the 1995 Kobe, Japan, earthquake determined from strong motion, teleseismic, and geodetic data, *J. Phys., Earth*, **44**, 489-503.

Yamamoto, H., K. Yamamoto, N. Kato, T. Hirasawa and Y. Iio, 1990: In situ stresses in the epicentral area of the Naganoken-Seibu earthquake of 1984 (II), *Prog. Abst. Seism. Soc. Japan*, 1990, No. 1, 24 (in Japanese).

Yamamoto, K., 1980: Theoretical determination of effective elastic constants of composite and its application to seismology, *Doctoral thesis*, Tohoku Univ., pp. 199.

Yamamoto, K., 1995a: Strength distribution of microfracture elements in granites under compression test, *Proc. 3rd SEGJ/SEG Symp.*, 327-334.

Yamamoto K., 1995b: The rock property of in-situ stress memory: Discussions on its mechanism. In Matsuki & Sugawara (eds.), *Proc. Int. Work Shop on Rock Stress Meas. at Great Depth*, Tokyo, 1995, 46-51.

Yamamoto, K., 1998: Estimation of fracture stress for intact rocks and possibility of long-term earthquake prediction, *Zisin 2*, **50**, Sup. 169-180 (in Japanese with English abstract).

Yamamoto, K., 1999: A model for fracturing process of intact rocks under axial loading of compression: The size-effect on strength for fracture of specimens, IUGG99, Birmingham, ST1/W12.

Yamamoto, K., M. Kosuga, and T. Hirasawa, 1981: A theoretical method for determination of effective elastic constants of isotropic composites, *Sci. Rep. Tohoku Univ., Ser. 5, Geophysiscs*, **28**, 47-67.

Yamamoto K., Y. Kuwahara, N. Kato and T. Hirasawa, 1990: Deformation rate analysis: A new method for in situ stress estimation from inelastic deformation of rock samples under uni-axial compressions, *Tohoku Geophys. J (Sci. Rep. Tohoku Univ., Ser 5)*, **33**, 127-147.

Yamamoto, K., H. Yamamoto, and Y. Yabe, 1997: Relation of in-situ stress field to seismic activity as inferred from the stresses measured on core samples, In K. Sugawara and Y. Obara (ed.), Rock Stress, A.A. Balkema, 375-380.

Yamamoto, K., Y. Yabe, and N. Sato, 1998: Stresses at sites close to the Nojima earthquake fault estimated from core samples: I, *Prog. Abst. Seism. Soc. Japan*, 1998 Fall Meeting, B13.

Yamamoto K., N. Sato, and Y. Yabe, 1999: Stress state around the Nojima fault estimated by core measurement, Proc. Int. W/S on the Nojima fault core and borehole data analysis, Nov. 22-23, '99, Tsukuba, Japan, GSJ Int. Rep. EQ/00/1, USGS Open-file Rep., 00-129, 239-246.

Yamamoto, K. and Y. Yabe, 2000: Stresses at sites close to the Nojima fault measured on boring core samples, *Island Arc*, in press.

Yoshida, S., K. Koketsu, B. Shibazaki, T. Sagiya, T. Kato, and Y. Yoshida, 1996: Joint inversion of near- and far-field waveforms and geodetic data for the rupture process of the 1995 Kobe earthquake, *J. Phys. Earth*, **44**, 437-454.

Zoback M. D. *et al.*, 1987: New evidence on the state of stress of the San Andreas fault system, *Science*, **238**, 1105-1111.

Zoback, M.D., and J.H. Healy, 1992: In situ stress measurements to 3.5 km depth in the Cajon Pass Scientific Research Borehole: Implications for the mechanics of crustal faulting, *J. Geophys. Res.*, **97**, 5039-5057.